J|A|C|S
ARTICLES
Published on Web 07/27/2002

X-ray Crystal Structures of Reduced Rubrerythrin and Its Azide Adduct: A Structure-Based Mechanism for a Non-Heme Diiron Peroxidase

Shi Jin,[†] Donald M. Kurtz, Jr.,*[,†] Zhi-Jie Liu,[‡] John Rose,[‡] and Bi-Cheng Wang[‡]

Contribution from the Departments of Chemistry and Biochemistry & Molecular Biology, Center for Metalloenzyme Studies and Georgia X-ray Crystallography Center, University of Georgia, Athens, Georgia 30602

Received April 18, 2002

Abstract: Rubrerythrin (Rbr) is a 44-kDa homodimeric protein, found in many air-sensitive bacteria and archaea, which contains a unique combination of a rubredoxin-like [Fe(SCys)$_4$] site and a non-sulfur, oxo/dicarboxylato-bridged diiron site. The diiron site structure resembles those found in O_2-activating diiron enzymes. However, Rbr instead appears to function as a hydrogen peroxide reductase (peroxidase). The diferrous site in all-ferrous Rbr (Rbr_{red}) shows a much greater reactivity with H_2O_2 than does the diferric site in all-ferric Rbr (Rbr_{ox}), but only the latter structure has been reported. Here we report the X-ray crystal structures of the recombinant Rbr_{red} from the sulfate reducing bacterium, *Desulfovibrio vulgaris*, as well as its azide adduct ($Rbr_{red}N_3$). We have also redetermined the structure of Rbr_{ox} to a higher resolution than previously reported. The structural differences between Rbr_{ox} and Rbr_{red} are localized entirely at the diiron site. The most striking structural change upon reduction of the diferric to the diferrous site of Rbr is a 1.8-Å movement of one iron away from a unique glutamate carboxylate ligand and toward a trans-disposed histidine side chain, which replaces the glutamate as a ligand. This movement increases the inter-iron distance from 3.3 to 4 Å. $Rbr_{red}N_3$ shows this same iron movement and His→Glu ligand replacement relative to Rbr_{ox}, and, in addition, an azide coordinated to the diiron site in a cis μ-1,3 fashion, replacing two solvent ligands in Rbr_{red}. Relative to those in O_2-activating enzymes, the bridging carboxylate ligation of the Rbr diiron site is less flexible upon diferric/diferrous interconversion. The diferrous site is also much more rigid, symmetrical, and solvent-exposed than those in O_2-activating enzymes. On the basis of these unique structural features, a mechanism is proposed for facile reduction of hydrogen peroxide by Rbr involving a cis μ-η^2 H_2O_2 diferrous intermediate.

Introduction

A protein containing a unique combination of an [Fe(SCys)$_4$] site and a non-sulfur, oxo-bridged diiron site was first isolated from the anaerobic sulfate-reducing bacterium, *Desulfovibrio vulgaris*.[1] At the time of its initial isolation, this protein had no known function and was, therefore, given the trivial name rubrerythrin (Rbr), a contraction of rubredoxin and hemerythrin, which were the prototypical proteins containing the respective iron sites listed above. A subsequent X-ray crystal structure of recombinant oxidized (all-ferric) *D. vulgaris* Rbr (Rbr_{ox}) confirmed the initial spectroscopic identifications of these iron sites.[2] More than a dozen Rbr homologues or their genes have since been identified from a variety of air-sensitive bacteria and archaea.[3] Within the past few years, Rbr has been implicated as one component of a novel oxidative stress protection system in these microorganisms.[4] Both in vivo[5−7] and in vitro[3,8,9] evidence indicates that Rbr can function as a hydrogen peroxide reductase (peroxidase) (reaction 1):

$$2e^- + 2H^+ + H_2O_2 \rightarrow 2H_2O \qquad (1)$$

Candidates for physiological electron donors in Rbr-catalyzed reaction 1 include Fe^{2+}, rubredoxin, and flavoprotein NADH: acceptor oxidoreductases.[3,8−10] Kinetics results on wild-type and site-directed variant Rbrs are consistent with a mechanism for reaction 1 in which the diferrous site of Rbr rapidly reduces

* To whom correspondence should be addressed at the Department of Chemistry. Fax: (706) 542-9454. E-mail: kurtz@chem.uga.edu.
[†] Department of Chemistry and Center for Metalloenzyme Studies.
[‡] Department of Biochemistry & Molecular Biology and Georgia X-ray Crystallography Center.

(1) LeGall, J.; Prickril, B. C.; Moura, I.; Xavier, A. V.; Moura, J. J. G.; Huynh, B. M. *Biochemistry* **1988**, *27*, 1636−1642.
(2) deMaré, F.; Kurtz, D. M., Jr.; Nordlund, P. *Nat. Struct. Biol.* **1996**, *3*, 539−546.
(3) Coulter, E. D.; Shenvi, N. V.; Beharry, Z.; Smith, J. J.; Prickril, B. C.; Kurtz, D. M., Jr. *Inorg. Chim. Acta* **2000**, *297*, 231−234.
(4) Kurtz, D. M., Jr.; Coulter, E. D. *Chemtracts, Inorg. Chem.* **2001**, *14*, 407−435.
(5) Alban, P. S.; Popham, D. L.; Rippere, K. E.; Krieg, N. R. *J. Appl. Microbiol.* **1998**, *85*, 875−882.
(6) Alban, P. S.; Krieg, N. R. *Can. J. Microbiol.* **1998**, *44*, 87−91.
(7) Lumppio, H. L.; Shenvi, N. V.; Summers, A. O.; Voordouw, G.; Kurtz, D. M., Jr. *J. Bacteriol.* **2001**, *183*, 101−108.
(8) Coulter, E. D.; Shenvi, N. V.; Kurtz, D. M., Jr. *Biochem. Biophys. Res. Commun.* **1999**, *255*, 317−323.
(9) Coulter, E. D.; Kurtz, D. M., Jr. *Arch. Biochem. Biophys.* **2001**, *394*, 76−86.
(10) Bonomi, F.; Kurtz, D. M., Jr.; Cui, X. *J. Biol. Inorg. Chem.* **1996**, *1*, 67−72.

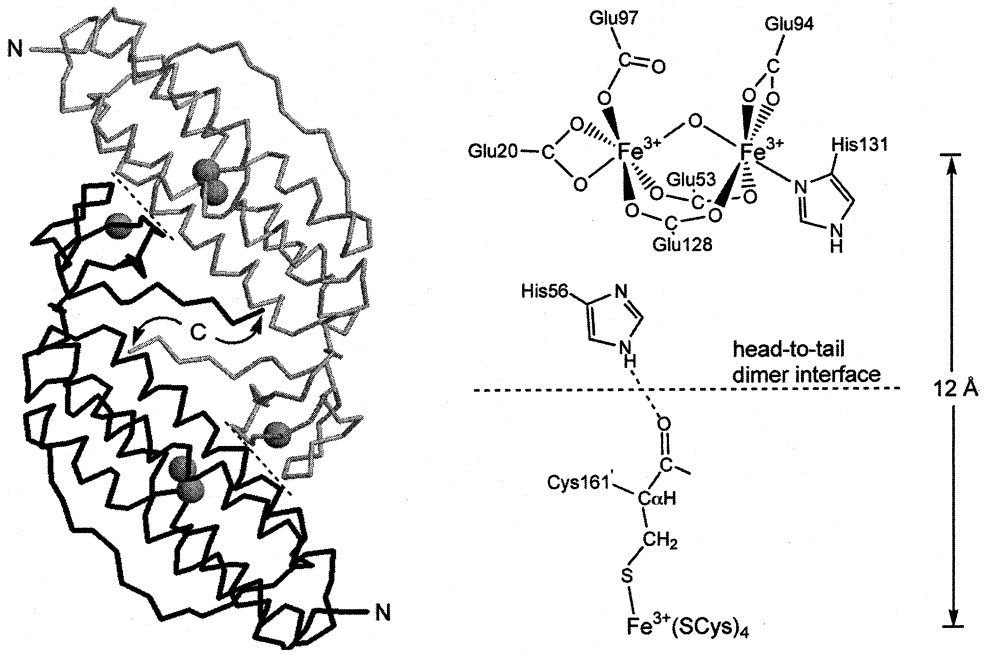

Figure 1. (Left) Protein backbone tracing of the *D. vulgaris* Rbr "head-to-tail" dimer viewed along its two-fold rotational axis drawn using RASMOL[13] and the published X-ray crystal structure coordinates (PDB 1RYT).[2] Iron atoms are represented as spheres, amino (N) and carboxyl (C) termini are labeled, and dashed lines indicate subunit interface regions between the [Fe(SCys)$_4$] and diiron sites. (Right) Schematic structure of the diiron site in *D. vulgaris* Rbr$_{ox}$, showing its proximity to the [Fe(SCys)$_4$] site across the head-to-tail dimer interface.

H_2O_2 and the [Fe(SCys)$_4$] site funnels electrons from the exogenous donors to the diiron site.[3,4] The reduced (all-ferrous) Rbr (Rbr$_{red}$) reacts with H_2O_2 on the millisecond time scale or faster, whereas its reaction with O_2 is orders of magnitude slower (several minutes).[3,8] Rbr$_{ox}$, on the other hand, shows little or no reactivity with hydrogen peroxide and no detectable catalase activity (i.e., catalysis of hydrogen peroxide disproportionation).[11]

The relatively sluggish reaction of Rbr$_{red}$ with O_2 is somewhat puzzling, because the diiron-ligating amino acid sequence of Rbr[2] is homologous to those in a class of enzymes in which the diiron sites are known to rapidly (millisecond time scale) activate O_2 for oxidation of another substrate or cofactor. These enzymes include ribonucleotide reductase R2 subunit (RNR−R2) and methane monooxygenase hydroxylase (MMOH).[12] One possible source of the difference in dioxygen reactivity may lie in an unanticipated ligation feature of the diiron site in Rbr$_{ox}$, which is shown in Figure 1.[2]

The diiron structural motif in the O_2-activating enzymes typically consists of a four-helix bundle that supplies six protein ligands, four carboxylates (from Asp or Glu), and two histidyl imidazoles within a pair of D/EX$_{29-37}$EX$_2$H sequences.[12] On the basis of this characteristic diiron-ligating sequence motif, both His131 and His56 in *D. vulgaris* Rbr had been predicted to furnish ligands to the diiron site.[14] However, the crystal structure of the diferric site in Rbr$_{ox}$ showed that, while His131Nδ is indeed a ligand, the Nδ of His56 is 4.2 Å away from the nearest iron, i.e., too far away to be a ligand. Instead, Glu97, which has no structural homologue in the O_2-activating diiron enzymes, but which is conserved in all known Rbrs,[3] provides a fifth carboxylate ligand (Fe−Oϵ1Glu 2.1 Å) that is trans-disposed relative to the His56 "nonligand". The His56NϵH is hydrogen-bonded to the carbonyl of a cysteine residue, whose Sγ provides a ligand to the [Fe(SCys)$_4$] site across the subunit interface of the "head-to-tail" dimer. This subunit interface between the [Fe(SCys)$_4$] and diiron domains, shown in Figure 1, provides the closest approach of the two metal sites (∼12 Å) in the crystal structure and is, therefore, presumed to be the principal route of electron transfer between these sites.

Redox-induced His56↔Glu97 ligand switching at the Rbr diiron site had been suggested[2] and was supported by a crystal structure of a Glu97Ala variant.[15] However, no crystal structure of Rbr$_{red}$ has been reported.[16] We now report the X-ray crystal structure of recombinant *D. vulgaris* Rbr$_{red}$ and its azide adduct (Rbr$_{red}$N$_3$). We have also redetermined the structure of recombinant *D. vulgaris* Rbr$_{ox}$ to a higher resolution than the previously published structure.[2] The redox-induced structural changes and the azide binding mode provide a basis for delineating the nature and selectivity of the dioxygen vs hydrogen peroxide reactivities of this unique non-heme diiron protein.

Experimental Section

Protein Expression, Purification, and Crystallization. Recombinant *Desulfovibrio vulgaris* Rbr was overexpressed in *Escherichia coli*, iron-constituted, and purified as previously described,[3,18] but with one additional purification step. After the gel filtration, Rbr was loaded onto a Hitrap-Q (Amersham Pharmacia Biotech) column pre-

(11) Pierik, A. J.; Wolbert, R. B. G.; Portier, G. L.; Verhagen, M. F. J. M.; Hagen, W. R. *Eur. J. Biochem.* **1993**, *212*, 237−245.
(12) Kurtz, D. M., Jr. *J. Biol. Inorg. Chem.* **1997**, *2*, 159−167.
(13) Sayle, R.; Milner-White, E. J. *Trends Biochem. Sci.* **1995**, *20*, 374−376.
(14) Kurtz, D. M., Jr.; Prickril, B. C. *Biochem. Biophys. Res. Commun.* **1991**, *181*, 337−341.
(15) deMaré, F.; Nordlund, P.; Gupta, N.; Shenvi, N. V.; Cui, X.; Kurtz, D. M., Jr. *Inorg. Chim. Acta* **1997**, *263*, 255−262.
(16) A considerable body of evidence (summarized in ref 4) indicates that the recently reported Zn,Fe rather than diiron site in *D. vulgaris* Rbr (ref 17) is an artifact of isolation and/or crystallization.
(17) Sieker, L. C.; Holmes, M.; Le Trong, I.; Turley, S.; Liu, M.-Y.; LeGall, J.; Stenkamp, R. E. *J. Biol. Inorg. Chem.* **2000**, *5*, 505−513.
(18) Gupta, N.; Bonomi, F.; Kurtz, D. M., Jr.; Ravi, N.; Wang, D. L.; Huynh, B. H. *Biochemistry* **1995**, *34*, 3310−3318.

equilibrated with 25 mM 3-(*N*-morpholino)propanesulfonic acid (MOPS), pH 7.3. The fraction containing Rbr (monitored as A_{280}) was eluted with the same buffer, concentrated to ~1 mM in Rbr homodimer in a Centricon (Amicon) cell, and stored at −80 °C until further use. Oxidized Rbr (Rbr_{ox}) solutions prepared in this fashion were used for all crystallizations. Crystals of Rbr_{ox} were grown by the hanging drop method as previously described,[2] except that 12% glycerol was added to the reservoir. Deep red crystals were observed within hours of setting up the crystallization, and these were allowed to continue growing for 2−3 days. Rbr_{ox} crystals ~0.3 × 0.2 × 0.2 mm^3 in size were mounted in 20-μm cryoloops and flash-frozen to 95 K in a nitrogen cryostream. To obtain reduced (all ferrous) Rbr (Rbr_{red}) crystals, a reducing reservoir solution containing 15% PEG 1450, 10 mM NADH, and 5 mM sodium dithionite in 0.1 M tris(hydroxymethyl)aminomethane (Tris), pH 8.5, was degassed and flushed with argon using a vacuum manifold. Crystallization was carried out in an anaerobic chamber using the hanging drop method. Five microliters of Rbr_{ox} solution was mixed with an equal volume of the reducing reservoir buffer. Neither the sodium dithionite nor the NADH in the reservoir buffer noticeably reduced the iron sites in Rbr_{ox}, as judged by retention of the red color in the mixed solution. To this mixture was added 1 μL of 0.4 mM BenC, an Fe−S, FAD-containing NADH oxidoreductase[19] that has been demonstrated to catalyze reduction of Rbr_{ox} by NADH.[3] Upon mixing, the deep red color of the solution quickly bleached to colorless, indicating full reduction of Rbr. Colorless, diffraction-quality Rbr_{red} crystals were observed within 2 days using a Stender Dish (Hampton Research Co.) for a better seal. For mounting, Rbr_{red} crystals and a dewar of liquid nitrogen were brought into an argon-purged glovebag using the protruding eyepiece of a microscope for visualization. The crystals (~0.3 × 0.2 × 0.2 mm^3) were mounted on cryoloops, rinsed with mineral oil (which had been degassed by argon flow), flash-frozen, and stored in liquid nitrogen. Colorless crystals of the Rbr_{red} azide adduct ($Rbr_{red}N_3$) (~0.3 × 0.2 × 0.2 mm^3) were obtained and mounted using the same methods described for Rbr_{red}, except that the reservoir buffer contained 25 mM MOPS, pH 7.3, and 150 mM sodium azide in place of the Tris.

Data Collection and Refinement. All data were collected on a Rigaku Raxis IV detector using Cu Kα X-rays generated on a Rigaku RU200 rotating anode in the Georgia X-ray Crystallography Center at the University of Georgia. The temperature of the crystals was maintained at 95 K throughout data collection in a cryostream of nitrogen gas. For Rbr_{ox} and Rbr_{red} crystals, data were collected using a total of 360 one-degree oscillations for 5-min exposures. For $Rbr_{red}N_3$ crystals, a total of 180 one-degree oscillations were used. The data were indexed, integrated using DENZO, and scaled using SCALEPACK.[20] The molecular replacement calculations and refinement steps were carried out using CNS 1.0,[21] and model rebuilding was performed in O.[22] Drawings were generated using MOLSCRIPT[23] output rendered by Raster3D,[24] unless otherwise noted.

Rbr_{ox}. The Rbr_{ox} structure was determined by molecular replacement, using the published Rbr_{ox} coordinates in PDB code 1RYT as the search model with all solvent molecules, including the oxo bridge at the diiron site, removed. The coordinate file of the search model with all solvent molecules (including the oxo bridge at the diiron site) removed was converted to a format suitable for CNS. The correlation coefficient of best solution after cross-rotation and translation searches was 0.758 and $\theta_1 = 157.09$, $\theta_2 = 0.23$, $\theta_3 = 203.25$, $x = 24.43$, $y = -0.02$, $z = 49.87$. At this point, 8% of the reflections were excluded to monitor the refinement. The full resolution range of data was used in rigid-body refinement. The starting *R* factor was lowered from 0.351 to 0.347, and R_{free} was 0.339, with no significant change. After refinement by conjugate gradient energy minimization, *R* (R_{free}) dropped to 0.301 (0.317). Because simulated annealing refinement did not lower either *R* factor, the model generated in minimization refinement was used to calculate a composite omit map ($2F_o - F_c$). After this first round of refinement, both the model and the electron density map were displayed in O, and disoriented side chains of several residues were manually rebuilt to better fit into the electron density map. The N-terminal methionine was not observed in the map and was assumed to be disordered. The new model was refined by minimization and simulated annealing, which lowered *R* (R_{free}) to 0.295 (0.307). Grouped *B*-factor refinement followed by individual *B*-factor refinement further reduced *R* (R_{free}) to 0.268 (0.278). At this point, 129 water molecules with peak heights above 3σ were picked by difference Fourier analysis and refined as oxygen atoms, which decreased *R* (R_{free}) to 0.227 (0.241). The occupancies for all atoms were constrained to 1.0 (excluding atoms in multiconformers of Arg54, discussed below) throughout refinement; *B*-factor values, therefore, reflect both thermal motion and disorder. Another minimization refinement reduced *R* (R_{free}) to 0.218 (0.234), and this new model was checked and adjusted against a composite omit map in O. A third round of refinement using an iterative process, during which 102 new water molecules were picked, decreased *R* (R_{free}) to 0.193 (0.214). The composite omit map at this point did not match the side-chain and backbone atoms of residues Gly78 and Ile79 from the model, so these residues were manually rebuilt with a *cis*-peptide bond connecting them. An obvious electron density connecting Fe1 and Fe2 at the diiron site and corresponding to the oxygen bridge in 1RYT was manually fitted as a water molecule. The electron density map at the Arg54 side chain was initially interpreted as one conformation with two water molecules located nearby. However, a better visual fit was obtained as two alternative side-chain conformations, so these two water molecules were deleted, and the alternate conformation of Arg54 was fitted to the map. The final round of refinement was carried out including minimization, grouped and individual *B*-factors, and simulated annealing. The parameter file of the *cis*-peptide bond between Gly78 and Ile79, and the topology file, including the multiple conformers of Arg54, were used during the final refinement. The final *R* (R_{free}) was 0.190 (0.210). The coordinates of the final model, including 230 water molecules per protein subunit, were confirmed using a new composite omit map in O.

Rbr_{red}. Difference Fourier analysis was used to refine the structure of Rbr_{red}. The initial Rbr_{red} model used the coordinates for Rbr_{ox} obtained just after the third round of refinement described above and before the third round of rebuilding in O with solvent coordinates removed. After rigid body refinement, *R* (R_{free}) decreased from 0.353 (0.336) to 0.342 (0.324). The subsequent refinement route followed that described above for Rbr_{ox}, except that simulated annealing refinement was omitted if it did not improve the model. After the first round of refinement, *R* (R_{free}) decreased to 0.303 (0.322). The first composite omit map showed a large unassigned electron density at the diiron site, which was connected to the electron densities of residues Glu20, Glu53, Glu128, and His 56. However, the closest iron to this large electron density, Fe1, had been placed in a relatively much weaker electron density nearby with no connection to other residues. Fe1 was, therefore, manually moved into the center of the large density, and the smaller density was assigned to a water molecule. The correctness of this repositioning of Fe1 was later confirmed in the anomalous difference Fourier map of Rbr_{red} (described below). After the second round of refinement with the first shell of 150 water molecules picked, *R* (R_{free}) decreased to 0.212 (0.226). A simulated annealing composite omit map ($2F_o - F_c$) was calculated, omitting residues Gly78 and Ile79.

(19) Karlsson, A.; Beharry, Z. M.; Eby, D. M.; Coulter, E. D.; Neidle, E. L.; Kurtz, D. M., Jr.; Eklund, H.; Ramaswamy, S. *J. Mol. Biol.* **2002**, *318*, 261−272.
(20) Otwinowski, Z. In *Proceedings of the CCP4 weekend*; Sawyer, L., Isaacs, N., Bailey, S., Eds.; Daresbury Laboratories: Warrington, UK, 1993; pp 56−62.
(21) Brünger, A. T.; Adams, P. D.; Clore, G. M.; DeLano, W. L.; Gros, P.; Grosse-Kunstleve, R. W.; Jiang, J. S.; Kuszewski, J.; Nilges, M.; Pannu, N. S.; Read, R. J.; Rice, L. M.; Simonson, T.; Warren, G. L. *Acta Crystallogr. D Biol. Crystallogr.* **1998**, *54*, 905−921.
(22) Jones, T.; Zou, J.; Cowan, S.; Kjeldgaard, M. *Acta Crystallogr. A* **1991**, *47*, 110−119.
(23) Kraulis, P. J. *J. Appl. Crystallogr.* **1991**, *24*, 946−950.
(24) Merritt, E. A.; Murphy, M. E. P. *Acta Crystallogr. D* **1994**, *50*, 869−873.

Table 1. Data Collection and Refinement Statistics

parameter	Rbr_{ox}	Rbr_{red}	$Rbr_{red}N_3$
A. Data Collection and Processing Statistics			
temperature (K)	95	95	95
unit cell dimensions (Å)			
a	48.9	48.5	48.3
b	80.6	80.0	80.1
c	100.1	100.1	100.2
maximum resolution (Å)	1.69	1.63	1.64
total reflections	257 523	273 708	133 046
unique reflections	21 164	22 434	21 509
completeness[a] (%)	93.7	90.6	88.6
R_{merge}[b] (%)	6.5 (20.9)	7.7 (18.3)	5.8 (18.6)
R_{ano}[c] (%)	6.5 (20.9)	7.7 (18.4)	5.8 (18.6)
$\langle I\rangle/\langle\sigma(I)\rangle$	44.8	48.8	46.5
B. Refinement Statistics			
resolution range for refinement	25.95−1.69	25.75−1.63	23.37−1.64
R_{work} (%)	18.96	18.35	17.80
R_{free}[d] (%)	21.02	20.48	20.23
number of water molecules	230	271	262
number of azide ions			2
rmsd's from ideality[e]			
bond lengths (Å)	0.005	0.004	0.005
bond angles (deg)	1.1	1.1	1.1
dihedral angles (deg)	19.1	19.3	19.4
improper angles (deg)	0.73	0.75	0.73
Wilson *B*-value (Å^2)	24.0	21.5	18.9
mean *B*-value (Å^2)	22.3	18.9	17.5
coordinate error[f] (Å)	0.19	0.18	0.17
Ramachandran plot[g]			
residues in most favored regions (%)	93.5	92.9	92.9
residues in additional allowed regions (%)	6.5	7.1	7.1
residues in generously allowed regions (%)	0	0	0
residues in disallowed regions (%)	0	0	0

[a] Values in parentheses correspond to the resolution shell. [b] $R_{merge} = \sum(|I - \langle I\rangle|)/\sum\langle I\rangle$. [c] Anomalous difference, $R_{ano} = \sum(|\langle I_+\rangle - \langle I_-\rangle|)/\sum\langle I\rangle$. [d] Calculated with 8% of the complete data set excluded from refinement. [e] Stereochemical check was made using CNS. [f] Estimated coordinate error from the Luzatti plot. [g] Ramachandran plot was calculated using PROCHECK.[27]

Another 124 water molecules were assigned, including two which appeared to be ligands to the iron atoms of the diiron site. After this third round of refinement, *R* (R_{free}) decreased to 0.185 (0.205). After the third model rebuilding, the total number of water molecules was reduced to 271. Two of these removed water molecules were due to the alternate conformation of Arg54. A final round of refinement gave no significant improvement of the model; the final *R* (R_{free}) factor was 0.184 (0.205).

$Rbr_{red}N_3$. Refinement of $Rbr_{red}N_3$ structure was performed similarly to that described for Rbr_{red}. The initial model used the third coordinate file of Rbr_{red} that had been written out from O with solvent coordinates removed. The parameter file for the *cis*-peptide bond between Gly78 and Ile79 was used from the first step. This initial model gave *R* (R_{free}) of 0.307 (0.299). After the first round of refinement, *R* decreased to 0.286, but R_{free} increased slightly to 0.303. The first composite omit map showed a rod-shaped electron density connecting the two irons at the diiron site. Since published EPR/ESEEM evidence indicates that azide perturbs the ferrous ions at the diiron site,[18,25] the rod-shaped electron density was modeled as a μ-1,3 bridging azide ion. The topology and parameter files for the azide ion were obtained from Kleywegt's HIC-UP server.[26] The N1−N2−N3 angle of the coordinated azide was 173°, and this angle was restrained during subsequent refinement. During the second round of refinement, 144 water molecules were picked, and *R* (R_{free}) decreased to 0.213 (0.224). Arg54 refined as two conformers during the next round of refinement. Another 121 waters were picked, and *R* (R_{free}) decreased to 0.198 (0.208). During the third model rebuilding, a water molecule at the protein surface was remodeled as an azide ion, based on the rod shape of the corresponding electron density. A final round of refinement was carried out, after which *R* (R_{free}) decreased to 0.178 (0.203). The final model had 262 water molecules and 2 azide ions per protein subunit.

All Structures. Data collection and refinement statistics for all three structures are summarized in Table 1. Some side-chain atoms of Lys2, Lys5, Lys11, Lys35, Leu69, Glu151, and Gln152 in all three models were disordered, as evidenced by incomplete electron densities in the composite omit maps. In addition, some side-chain atoms of Glu111 and Arg119 were disordered in Rbr_{red} and $Rbr_{red}N_3$. All of these residues are located at the protein surface. The positions of the three irons in each structure were confirmed by anomalous difference Fourier maps. For each structure, a Hendrickson−Lattman coefficient was generated using an anomalous reflection file and the coordinate file from the final refinement, but with irons excluded from phase calculations. An anomalous difference Fourier map was then computed in CNS using data to 3.0-Å resolution. To examine differences between structures, $F_{obs}(Rbr_{red}N_3) - F_{obs}(Rbr_{red})$ electron density maps were calculated after removing solvent molecules from the models (including the two iron-ligating solvent molecules in Rbr_{red}). The atomic coordinates for Rbr_{ox}, Rbr_{red}, and $Rbr_{red}N_3$ have been deposited in the Protein Data Bank with accession numbers 1LKM, 1LKO, and 1LKP, respectively.

Results

Overall Structures. Crystals obtained for all three *D. vulgaris* Rbr forms examined in this work, Rbr_{ox}, Rbr_{red}, and $Rbr_{red}N_3$, belonged to space group *I*222, which is isomorphous with that published for the original *D. vulgaris* Rbr_{ox} crystal structure (PDB 1RYT).[2] Even though only homodimers have been detected for this Rbr in solution, all three forms of Rbr examined here crystallized as tetramers (as reported for the 1RYT

(25) Sturgeon, B. E.; Doan, P. E.; Liu, K. E.; Burdi, D.; Tong, W. H.; Nocek, J. M.; Gupta, N.; Stubbe, J.; Kurtz, D. M., Jr.; Lippard, S. J.; Hoffman, B. M. *J. Am. Chem. Soc.* **1997**, *119*, 375−386.
(26) Kleywegt, G. J.; Jones, T. A. *Acta Crystallogr. D Biol. Crystallogr.* **1998**, *54*, 1119−1131.

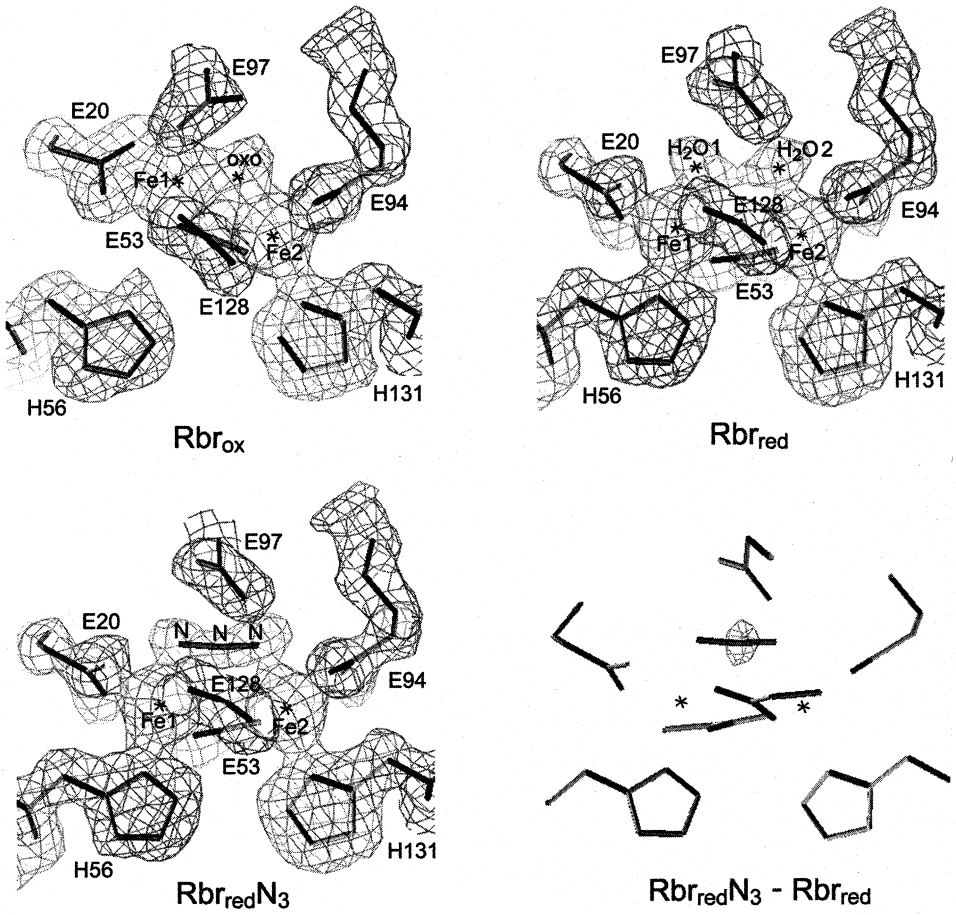

Figure 2. Final models and $2F_o - F_c$ composite omit maps contoured at 1.0σ at the diiron sites of Rbr_{ox} (top left), Rbr_{red} (top right), and $Rbr_{red}N_3$ (bottom left) and the final model of $Rbr_{red}N_3$ superimposed on the $[F_o(Rbr_{red}N_3) - F_o(Rbr_{red})]$ omit map contoured at 3.9σ at the diiron site (bottom right). Stars indicate positions of iron atoms and solvent oxygen ligands. Viewing perspective in all cases is approximately perpendicular to the Fe1- - -Fe2 axis with Glu128 in the foreground.

structure). The asymmetric unit contains one Rbr subunit, which is related to the remaining subunits of the tetramer by crystallographic two-fold axes. All three models have good stereochemistry, with low rmsd's from ideality in bond length and angles (cf. Table 1). Ramachandran plots from PROCHECK[27] showed no residues in disallowed regions, or even generously allowed regions. The overall structures of Rbr_{ox}, Rbr_{red}, and $Rbr_{red}N_3$ are all very similar to that of the published Rbr_{ox} (1RYT).[2] The corresponding residues in Rbr_{ox}, Rbr_{red}, and $Rbr_{red}N_3$ all have very similar conformations.

Both the diiron and $[Fe(SCys)_4]$ site structures are nearly identical in 1RYT vs Rbr_{ox}, with rmsd's of 0.24 Å for the diiron site (including residues 20, 53, 56, 94, 97, 128, and 131) and 0.14 Å for the $[Fe(SCys)_4]$ site (including residues 158,161, 174, and 177). Ordered water molecules near the diiron site and in a crevice exposing the diiron site to bulk solvent are in different positions in 1RYT and Rbr_{ox}. In 1RYT, an ordered water (water 1) is within hydrogen-bonding distance (2.8 Å) of the oxo bridge, and a second water farther away from the diiron site is within hydrogen-bonding distance (2.9 Å) of water 1. These two waters are not found in Rbr_{ox}, where several ordered waters that are >4 Å away from the oxo bridge are instead observed. The average Fe−O oxo bridge bond distances in both Rbr_{ox} and 1RYT (2.0 Å) are longer than, but only slightly outside of experimental error from, the 1.8 Å typical for diferric oxo/carboxylato-bridged complexes.[28] Resonance Raman spectroscopy, however, has unambiguously established the presence of an oxo bridge at the diiron site of *D. vulgaris* Rbr_{ox}.[29]

The overall rmsd's of Rbr_{ox} vs 1RYT, Rbr_{red} vs Rbr_{ox}, $Rbr_{red}N_3$ vs Rbr_{ox}, and $Rbr_{red}N_3$ vs Rbr_{red} are 0.86, 0.50, 0.50, and 0.31 Å, respectively. The better rmsd agreement of the Rbr_{red} and $Rbr_{red}N_3$ structures with that of Rbr_{ox} than with 1RYT may be due to the X-ray diffraction data being collected at room temperature for 1RYT vs 95 K for the three structures reported here. All three Rbr structures reported here have higher resolutions than that of 1RYT (2.1 Å) and reasonably low R and R_{free} factors (cf. Table 1). Subsequent comparisons are, therefore, confined to the three structures reported here. Furthermore, since no significant differences occur in the protein structures, we limit comparisons to the iron sites and their immediate environments.

Comparison of Rbr_{ox} and Rbr_{red} Diiron Sites. Figure 2 compares the $2F_o - F_c$ composite omit electron density maps and final models at the diiron sites of Rbr_{ox} and Rbr_{red}. The $2F_o - F_c$ composite omit electron density map of Rbr_{red} shows two peaks at the diiron site (Fe1, 19.7σ; Fe2, 21.1σ), which were of higher intensity than those in the Rbr_{ox} map (Fe1,

(27) Laskowski, R. A.; Macarthur, M. W.; Moss, D. S.; Thornton, J. M. *J. Appl. Crystallogr.* **1993**, *26*, 283−291.

(28) Kurtz, D. M., Jr. *Chem. Rev.* **1990**, *90*, 585−606.

(29) Dave, B. C.; Czernuszewicz, R. S.; Prickril, B. C.; Kurtz, D. M., Jr. *Biochemistry* **1994**, *33*, 3572−3576.

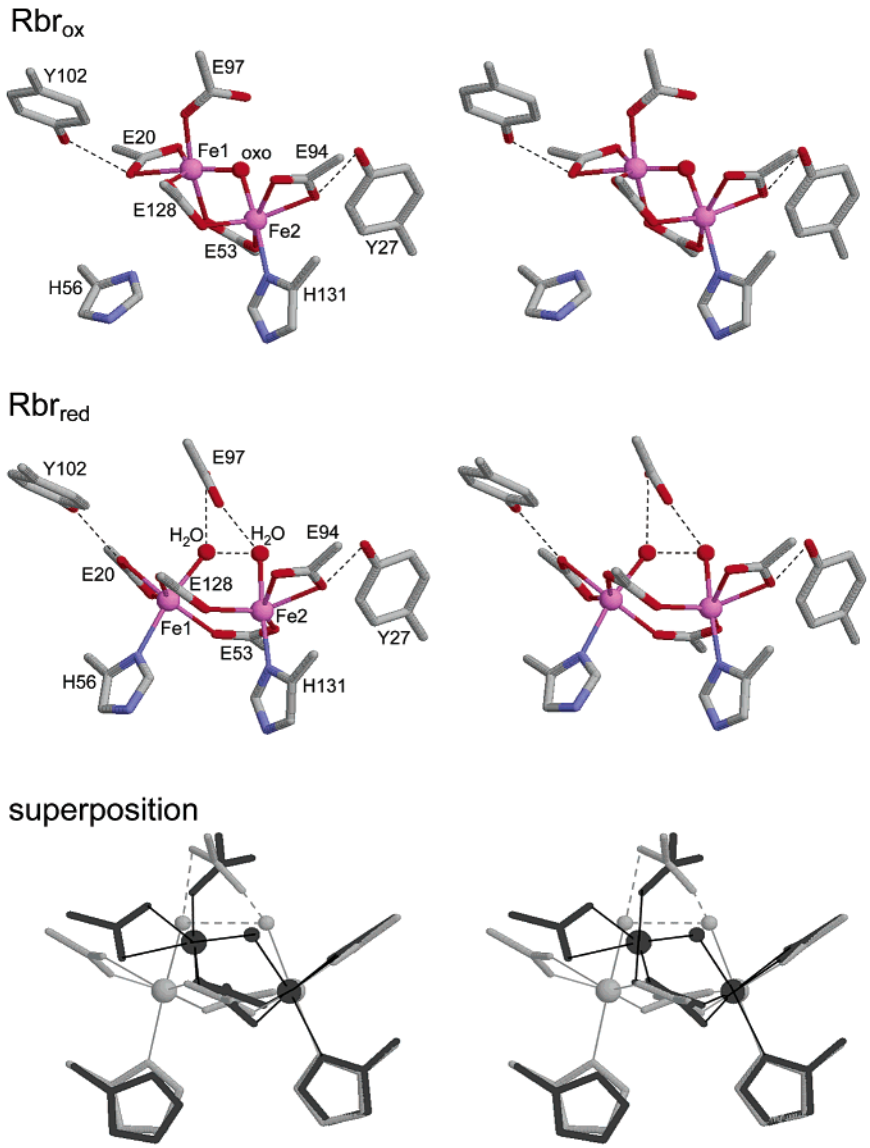

Figure 3. Stereoviews of diiron site structures in Rbr$_{ox}$ (top), Rbr$_{red}$ (middle), and superposition of the subunits (bottom, with Rbr$_{ox}$ darker shaded and Rbr$_{red}$ lighter shaded) in the region of the diiron sites. Tyrosine side chains in the second coordination spheres are shown in the top two views. Dashed lines indicate hydrogen bonds. For clarity, the glutamate β-carbons are not shown. Views are oriented so that the head-to-tail dimer interface is at the bottom and the protein crevice exposing the site to solvent is at the top. Drawings were generated using RASMOL[13] and coordinates reported in this work.

14.4σ; Fe2, 14.6σ), whereas the peak intensities of Fe3 at the [Fe(SCys)$_4$] sites were similar to each other (18.4σ in Rbr$_{red}$ and 17.9σ in Rbr$_{ox}$). These relative intensities are reflected in the respective *B*-factors (Å^2) of the three irons in Rbr$_{red}$ vs Rbr$_{ox}$, namely, Fe1, 12.4 vs 19.9; Fe2, 11.9 vs 18.4; and Fe3, 11.9 vs 14.3. The higher intensities in the composite omit maps and the significantly lower *B*-factors together indicate that the diiron site irons are more ordered in Rbr$_{red}$ than in Rbr$_{ox}$, perhaps reflecting a more rigid diferrous than diferric site.

Figure 3 shows the final models of the Rbr$_{ox}$ and Rbr$_{red}$ diiron sites and the best-fit superposition of the final Rbr$_{ox}$ and Rbr$_{red}$ subunit models in the region of the diiron sites. The two irons of the diiron site are labeled Fe1 (terminally ligated to by Glu20) and Fe2 (terminally ligated by Glu94). Both Fe1 and Fe2 in Rbr$_{red}$ are pseudo-octahedrally coordinated; each iron is ligated terminally by one bidentate glutamate, one histidine, and one solvent, and the irons are bridged by two bidentate glutamate ligands. The single largest structural change at the diiron site of Rbr$_{red}$ relative to Rbr$_{ox}$ is a 1.8-Å movement of Fe1 toward Nδ1 of His56. The imidazole ring of His56 has also moved 0.4 Å toward Fe1 upon conversion to Rbr$_{red}$. These movements have resulted in His56 replacing Glu97 as a ligand to Fe1 upon conversion of Rbr$_{ox}$ to Rbr$_{red}$ The Fe1−His56Nδ1 distance has shortened from 4.2 Å in Rbr$_{ox}$ to 2.3 Å in Rbr$_{red}$. The other side chains furnishing ligands to Fe1 have also moved significantly in Rbr$_{red}$ relative to their Rbr$_{ox}$ positions. The carboxyl plane of Glu97 has rotated by ~80° away from Fe1, resulting in ~1.4-Å movements of the Glu97 carboxylate oxygens from their Rbr$_{ox}$ positions. The carboxyl plane of Glu20 has rotated ~70° and moved 1.2 Å away from the original position of Fe1 in Rbr$_{ox}$, and the carboxyl planes of the bridging Glu53 and Glu128 ligands have both rotated 20−30° toward Fe1. Fe2, on the other hand, has moved only ~0.2 Å relative to its Rbr$_{ox}$ position, and no significant conformational changes or movements in Glu94 or His131, which furnish terminal ligands to Fe2, occur upon conversion to Rbr$_{red}$. The Fe1- - -Fe2 distance has elongated from 3.3 Å in Rbr$_{ox}$ to 4.0 Å in Rbr$_{red}$, and this elongation is accompanied by loss of the oxo bridge between

Fe1 and Fe2, which is replaced in Rbr_{red} by the two terminally ligated solvent molecules. The solvent oxygen ligands, O1 and O2, are 2.6 Å apart from each other, and presumably hydrogen-bonded to each other. This distance is longer than has been reported for the short hydrogen bond of the bridging $H_3O_2^-$ ion in dimetal complexes (O1- - -O2 < 2.5 Å).[30,31] For this reason and because of the identical Fe1−O1 and Fe2−O2 bond lengths (2.2 Å), we favor formulation of both solvent ligands as aqua rather than hydroxo or $H_3O_2^-$. Two aqua ligands would also result in an overall zero net charge on the diferrous site. If the nonligating Glu97 carboxylate is included, the overall charge becomes −1, which is identical to that on the Glu97-ligated, oxo-bridged diferric site of Rbr_{ox}. The Fe1, Fe2, and their solvent ligand oxygens form a slightly twisted trapezoid in Rbr_{red} with an Fe1−O1- - -O2−Fe2 torsion angle of 21°. The imidazole rings of the His56 and His131 ligands lie approximately parallel to this trapezoidal plane and trans to the respective solvent ligands, whereas the two bridging carboxylate ligands (from Glu53 and Glu128) lie on opposite sides of the trapezoidal plane.

An unusual structural feature of the Rbr diferric site, not noted previously, is that both iron atoms lie well out of the two bridging carboxylate planes, whereas these irons lie approximately in the planes of their respective bidentate terminal carboxylate ligands, as can be seen qualitatively in Figure 3. A measure of this out-of-plane geometry is the Fe1(2)−Oϵ1(2)−Cδ−Cγ torsion angle around the Cδ−Oϵ1(2) glutamate bonds. Placement of the irons in the carboxylate ligand planes, i.e., torsion angles of 180°, presumably optimizes σ bonding interactions. For the bridging Glu128 and Glu53, these angles range from 126° to 149°, compared to 176−180° for the terminal Glu20 and Glu94. Irons located significantly out of the bridging carboxylate planes have not been observed in other non-heme diiron proteins or synthetic oxo-bridged diferric complexes, except in those of a conformationally constrained dicarboxylate ligand.[32,33] The diiron location out of the bridging carboxylate planes in Rbr_{ox} is notable now because of its contrast to the diiron site in Rbr_{red}. A consequence of the movements of Fe1 and its ligands in Rbr_{red} is a shift of the Fe1−Fe2 axis nearly into the average plane of the two anti-disposed bridging carboxylates, as can be seen in Figures 3 and 4.

The diiron site in Rbr_{red} is thus more symmetric than that in Rbr_{ox}. In fact, as shown in Figure 4, the corresponding side chains and solvent providing the coordination spheres of Fe1 and Fe2 in Rbr_{red} can be nearly superimposed onto each other by a 180° rotation around an axis bisecting the Fe1- - -Fe2 and solvent ligand (O1- - -O2) axes. This pseudo-two-fold rotational symmetry extends out to the main chain atoms of the ligand residues, and even to two tyrosine side chains shown in Figure 3, which are hydrogen-bonded to the terminal carboxylates of Glu20 and Glu94. The two-fold rotational symmetry does not, however, extend to the carboxylate of the displaced Glu97, which lies on the Glu128 side of the Fe1- - -Fe2−(solvent ligand) trapezoid. Glu97Oϵ2 appears to form a strong hydrogen bond with the solvent oxygen ligand of Fe2 (Glu97Oϵ2- - -O2(solvent ligand) = 2.6 Å). The Glu97Oϵ1 may form a weaker hydrogen bond to the solvent oxygen ligand of Fe1 ((Glu97Oϵ1- - -O1(solvent ligand) = 2.9 Å).

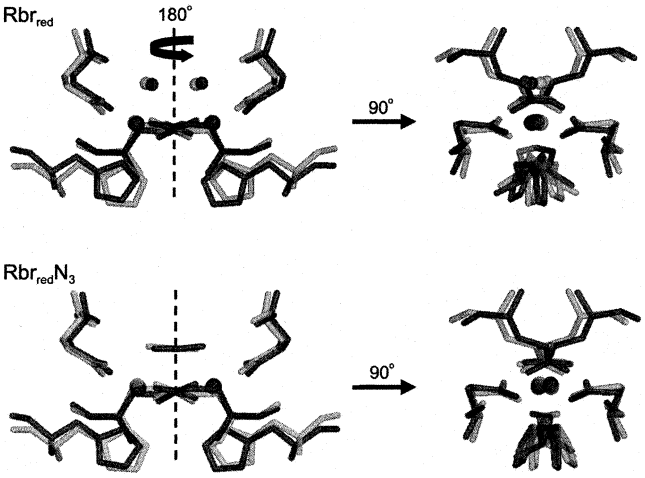

Figure 4. Views depicting the pseudo-two-fold rotational axes superimposing the Fe1 and Fe2 coordination spheres onto each other in Rbr_{red} (top) and $Rbr_{red}N_3$ (bottom). Lighter and darker shadings indicate structures before and after 180° rotations around the axis represented by the dashed line. The structures to the right of the "90°"-labeled arrows are the same as those to the left but rotated 90° around the dashed-line axis. Iron atoms and solvent are represented as larger and smaller spheres, respectively. Azide in $Rbr_{red}N_3$ is represented in wireframe above the Fe1- - -Fe2 axis.

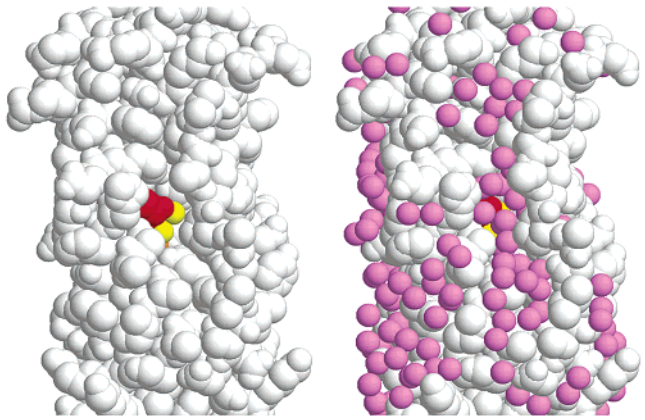

Figure 5. Space-filling stereoview of the Rbr_{red} four-helix bundle domain (long axis oriented vertically) showing the crevice exposing the diiron site. Iron atoms (orange) are barely visible directly underneath the solvent ligands, which are highlighted in yellow. Glu97 is highlighted in red. Right image shows ordered solvent molecules (purple). Drawing was generated using RASMOL.[13]

The Glu97Oϵ1 is also hydrogen-bonded to at least one of several ordered solvent molecules that occupy a crevice exposing the diiron site to bulk solvent (cf. Figure 5). The two His ligands also participate in distinctly different hydrogen-bonding interactions. As is the case for Rbr_{ox} (cf. Figure 1), His56Nϵ2 is hydrogen-bonded to the carbonyl of Cys161 across the subunit interfaces of the head-to-tail dimer in Rbr_{red}, whereas His131Nϵ2 is hydrogen-bonded to the side-chain carbonyl of Gln52. A conserved Arg residue (Arg26) lines the crevice leading to solvent, but its guanidinium group is too far away for direct interaction with any atoms of the diiron coordination sphere. In Rbr_{red}, an Arg26 guanidinium NH_2 is 5.8 Å from a Glu97 carboxylate oxygen, and these two atoms appear to be bridged by an intervening water molecule. A possible role for Arg26 is charge compensation for Glu97.

(30) Dong, Y. H.; Fujii, F.; Hendrich, M. P.; Keising, R. A.; Pan, G. F.; Randall, C. R.; Wilkinson, E. C.; Zang, Y.; Que, L., Jr.; Fox, B. G.; Kauffmann, K.; Münck, E. *J. Am. Chem. Soc.* **1995**, *117*, 2778−2792.
(31) Ardon, M.; Bino, A. *Struct. Bonding (Berlin)* **1987**, *65*, 1−28.
(32) Mizoguchi, T. J.; Lippard, S. J. *Inorg. Chem.* **1997**, *36*, 4526−4533.
(33) Mizoguchi, T. J.; Davydov, R. M.; Lippard, S. J. *Inorg. Chem.* **1999**, *38*, 4098−4103.

In contrast to the diiron site, the [Fe(SCys)$_4$] sites of Rbr$_{ox}$ and Rbr$_{red}$ show no significant structural differences. The rmsd between Rbr$_{red}$ and Rbr$_{ox}$ of the diiron ligating residues (Glu20, Glu53, Glu94, Glu97 Glu128, His56, and His 131) is 0.50 Å, whereas the analogous rmsd for the four residues (Cys158, Cys161, Cys174, and Cys177) furnishing ligands to the [Fe(SCys)$_4$] site is only 0.04 Å. The Fe−S distances are all 2.3 Å in both structures. Six N—H- - -S hydrogen bonds from backbone amides to these ligating Cys residues are also nearly superimposable in Rbr$_{ox}$ and Rbr$_{red}$. This hydrogen-bonding pattern was described previously to be very similar to that in rubredoxins.[2] Therefore, the unusually high reduction potential of the [Fe(SCys)$_4$] site in Rbr[18] relative to those of rubredoxins[34] cannot be attributed to significant alterations in either its first or second coordination spheres upon redox interconversion.[35]

Because of the movement of Fe1 toward His56 described above, the distance between Fe1 in one subunit and Fe3 (the [Fe(SCys)$_4$] site iron) in the other subunit of the head-to-tail dimer has decreased by 1.5 Å (from 12.4 to 10.9 Å) upon conversion of Rbr$_{ox}$ to Rbr$_{red}$. In contrast, the corresponding Fe2- - -Fe3 intersubunit distance has increased by 0.3 Å (from 11.9 to 12.2 Å).

Rbr$_{red}$N$_3$. Figure 2 shows the $2F_o - F_c$ electron density map and final model for the diiron site of Rbr$_{red}$N$_3$. The rmsd's between Rbr$_{red}$N$_3$ and Rbr$_{red}$ structures for the diiron ligating residues and Glu97 and for the four cysteine residues of the [Fe(SCys)$_4$] site are very low: 0.04 and 0.02, respectively. The only significant structural difference between Rbr$_{red}$N$_3$ and Rbr$_{red}$ is that the two solvent ligands at the diiron site of Rbr$_{red}$ are substituted by a μ-1,3 bridging azide ion in Rbr$_{red}$N$_3$. The positions of N1 and N3 of this bridging azide are very similar to those of the two water molecules in Rbr$_{red}$, but the intra-azide N1−N3 distance of 2.4 Å is significantly shorter than that between the two ligating water oxygens in Rbr$_{red}$ (2.6 Å). In the [F_{obs}(Rbr$_{red}$N$_3$) − F_{obs}(Rbr$_{red}$)] difference electron density map omitting all water molecules and azide ions (cf. Figure 2, lower right), the highest peak (6.0σ) at the diiron site is a positive difference density, the center of which is located near the position of the central nitrogen of the bridging azide. The average *B*-factor of the three bridging azide nitrogens (15.3 Å^2) is similar to that of the two solvent ligands in Rbr$_{red}$ (14.7 Å^2), although the *B*-factor of the central azide nitrogen, N2 (21.3 Å^2), is slightly higher than those of the two end nitrogens (12.8 and 11.9 Å^2 for N1 and N3, respectively). The remaining coordination sphere accommodates the substitution of solvent ligands by azide without significant structural changes compared to Rbr$_{red}$. The Fe1−Fe2 distance, 3.9 Å, is, within experimental error, identical to that in Rbr$_{red}$. The description of Fe1,Fe2 and their solvent ligands in Rbr$_{red}$ as a slightly twisted trapezoid also applies to Fe1,Fe2 and the bridging azide in Rbr$_{red}$N$_3$, which have an Fe1—N1- - -N3—Fe2 torsion angle of 18°. The Fe1−N1 and Fe2−N3 distances (2.2 Å) in Rbr$_{red}$N$_3$ are identical to each other. Analogously to Rbr$_{red}$, the Fe1 and Fe2 coordination spheres in Rbr$_{red}$N$_3$ can be nearly superimposed onto each other by a 180° rotation around a two-fold rotation axis passing through the central azide nitrogen (N2) and bisecting the Fe1−Fe2 axis (cf. Figure 4). The positioning of the Glu97 carboxylate in Rbr$_{red}$N$_3$ is also analogous to that in Rbr$_{red}$, sitting above and to the Glu128 side of the Fe1−Fe2−(μ-azido) trapezoidal plane. The two Glu97 carboxylate oxygens show longer and shorter distances to the two coordinated azide nitrogens that are similar to those to the respective coordinated solvent ligands in Rbr$_{red}$. The shorter of the two distances, Glu97Oϵ2- - -N3 at 2.5 Å, and the location of N3 close to the Glu97 carboxylate plane imply a hydrogen bond and, therefore, that either the carboxylate or the coordinated azide is protonated. The essentially identical Fe1−N1 and Fe2−N3 distances would suggest the former. As far as we are aware, the μ-1,3 bridging mode of azide has not been previously reported in either diferrous proteins or diferrous synthetic complexes, where azide invariably exhibits either terminal or μ-η^1 coordination.[36,37] On the basis of resonance Raman spectroscopy, a μ-1,3 bridging geometry was proposed for an azide adduct of the diferric site in stearoyl-acyl carrier protein Δ^9 desaturase.[38] Examples of μ-1,3 azide-bridged dicopper(II) complexes are available with cis Cu1—N1- - -N3—Cu2 torsion angles, i.e., similar to the geometry in Rbr$_{red}$N$_3$.[39−42] The slight deviation from linearity of the bridging azide in Rbr$_{red}$N$_3$ (N1−N2−N3 angle = 173°) is also observed in the μ-1,3 azide-bridged dicopper(II) complexes.

The non-Kramers EPR signal from a ferromagnetically coupled diferrous site previously observed for Rbr$_{red}$N$_3$, but not for Rbr$_{red}$,[18] can now be unambiguously attributed to alteration of the magnetic coupling and/or the zero-field splitting due to replacement of the two terminal solvent ligands in Rbr$_{red}$ by the bridging azide. The highly symmetrical Rbr$_{red}$N$_3$ diiron site also explains why only a single histidine ligand environment was observed when this non-Kramers EPR signal was probed by electron spin−echo envelope modulation (ESEEM) spectroscopy.[25]

Discussion

Structural Comparisons with Diiron Sites in Non-Heme O$_2$-Activating Enzymes. The comparisons made here attempt to highlight those structural differences that help explain the distinctive reactivity of the Rbr diiron site. As noted previously,[2] the oxo-bridged diferric site of Rbr is quite distinct from that of its namesake, hemerythrin,[43] most conspicuously in the histidine:carboxylate ligand ratio, which is reversed from 5:2 in hemerythrin to 2:5 in Rbr$_{ox}$. This structural distinction can now be extended to the reduced diiron sites. In addition to its higher histidine:carboxylate ligand ratio, changes in the diiron coordination sphere of hemerythrin upon reduction are relatively limited, essentially consisting only of protonation of the bridging oxo ligand. One of the iron atoms in diferrous hemerythrin is five-coordinate, whereas both iron atoms in Rbr$_{red}$ are six-

(34) Eidsness, M. K.; Burden, A. E.; Richie, K. A.; Kurtz, D. M., Jr.; Scott, R. A.; Smith, E. T.; Ichiye, T.; Beard, B.; Min, T.; Kang, C. *Biochemistry* **1999**, *38*, 14803−14809.
(35) None of the structures reported here shows evidence for the Asn160NdH- - -SgCys177 hydrogen bond reported in ref 17.
(36) Andersson, M. E.; Hogbom, M.; Rinaldo-Matthis, A.; Andersson, K. K.; Sjoberg, B. M.; Nordlund, P. *J. Am. Chem. Soc.* **1999**, *121*, 2346−2352.
(37) DeMunno, G.; Poerio, T.; Viau, G.; Julve, M.; Lloret, F.; Journaux, Y.; Riviere, E. *Chem. Commun.* **1996**, 2587−2588.
(38) Ai, J. Y.; Broadwater, J. A.; Loehr, T. M.; Sanders-Loehr, J.; Fox, B. G. *J. Biol. Inorg. Chem.* **1997**, *2*, 37−45.
(39) Mckee, V.; Zvagulis, M.; Dagdigian, J. V.; Patch, M. G.; Reed, C. A. *J. Am. Chem. Soc.* **1984**, *106*, 4765−4772.
(40) Sorrell, T. N.; O'Connor, C. J.; Anderson, O. P.; Reibenspies, J. H. *J. Am. Chem. Soc.* **1985**, *107*, 4199−4206.
(41) Kitajima, N.; Fujisawa, K.; Hikichi, S.; Morooka, Y. *J. Am. Chem. Soc.* **1993**, *115*, 7874−7875.
(42) Tuczek, F.; Bensch, W. *Inorg. Chem.* **1995**, *34*, 1482−1486.
(43) Stenkamp, R. E. *Chem. Rev.* **1994**, *94*, 715−726.

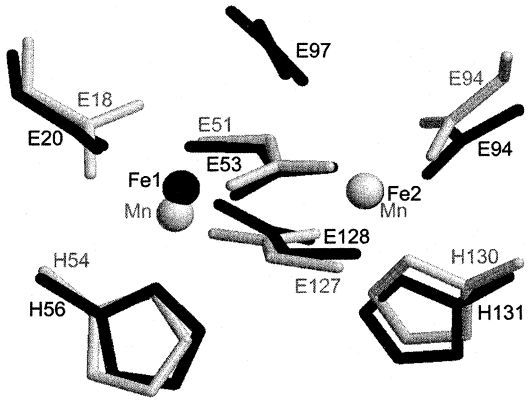

Figure 6. Superposition of Rbr_{red} (darker shaded) and *E. coli* Bfr (lighter shaded) subunits in the region of the diiron sites. Ligand side chains are shown in wireframe representation, and iron (Rbr) or manganese (Bfr) atoms are shown as spheres. Automated best-fit superposition of subunits was performed using SwissPDBviewer.[51] Drawing was generated using RASMOL.[13] and coordinates from this work (Rbr_{red}) and 1BCF (Bfr).[48]

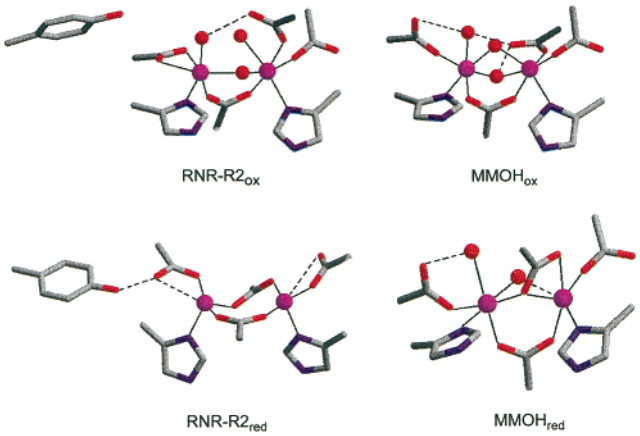

Figure 7. Diferric and diferrous site structures (labeled with "ox" and "red" subscripts, respectively) of *E. coli* RNR-R2 and *Methylococcus capsulatus* (Bath) MMOH. Ligand side chains are shown in wireframe, and irons and solvent ligands are shown as larger and smaller spheres, respectively. β-Carbons of glutamate residues are omitted for clarity. Dashed lines indicate hydrogen bonds. Structures were drawn using coordinates from PDB 1RIB ($RNR\text{-}R2_{ox}$),[54] 1XIK ($RNR\text{-}R2_{red}$),[53] 1MTY ($MMOH_{ox}$),[58] and 1FYZ ($MMOH_{red}$).[56]

coordinate. These structural distinctions in the hemerythrin vs Rbr diiron sites are reflected in their distinct reactivities. Diferrous hemerythrin has long been known to reversibly bind O_2, whereas Rbr has never been reported to do so. Conversely, hemerythrin has never been reported to show peroxidase activity, and its diferrous site is relatively slowly (minutes time scale) oxidized by excess hydrogen peroxide.[44] At least part of this difference in reactivity is also likely due to the hydrophobic O_2 binding pocket in hemerythrin vs the solvent-accessible diiron site in Rbr (cf. Figure 5).

The close structural resemblances of both the four-helix bundle domains and diiron site environments of Rbr to those of the iron storage proteins, ferritin (Ftn) and bacterioferritin (Bfr), have been noted previously.[2,45,46] An evolutionary relationship with Ftn's and Bfr's has even been suggested, despite their low overall amino acid sequence homology to the Rbr diiron domain.[47] Catalysis of Fe^{2+}(aq) oxidation by O_2, a characteristic reaction of Ftn and Bfr, proceeds at a "ferroxidase" center, which is a relatively unstable diiron binding site. *D. vulgaris* Rbr does, in fact, exhibit ferroxidase activity in vitro. However, in contrast to all known Ftn's and Bfr's, Rbr shows no evidence for formation of 24-mer structures or for binding the colloidal ferric oxyhydroxide product of the ferroxidase reaction. Conversely, Ftn and Bfr have not been reported to show peroxidase activity, and no known Ftn or Bfr contains the $[Fe(SCys)_4]$ domain found in Rbr's. Nevertheless, reinforcing the structural resemblance, Figure 6 shows that the best superposition of the four-helix bundle domains of Rbr_{red} and *E. coli* Bfr results in a remarkably close overlap of the Rbr diiron site iron atoms and their ligands with those of the ferroxidase center in Bfr, which was crystallized with Mn^{2+} occupying its dimetal binding site.[48] A notable distinction is that Bfr has no homologue to Glu97 in Rbr; the corresponding position in Bfr is occupied by a Gly residue. One proposed mechanism of iron incorporation into Bfr invokes migration of iron out of the dimetal site to the ferric/oxyhydroxide core.[49,50] Glu97 in Rbr may help localize movement of iron at the diiron site.

As noted in the Introduction, the Rbr_{ox} diiron site domain resembles those in the non-heme O_2-activating diiron enzymes, RNR-R2 and MMOH.[52−57] These latter diferric and diferrous site structures are shown in Figure 7, which may be compared with the corresponding Rbr structures in Figure 3. Common features of the diiron sites in Rbr, RNR-R2, and MMOH include a 2:4 histidine:carboxylate ligand ratio in the diferrous forms and solvent-derived oxygen bridges, either oxo (RNR−R2) or hydroxo/aqua (MMOH), in the diferric form, which are broken upon conversion to the diferrous forms.

Several other structural features, however, distinguish the primary coordination spheres of the Rbr diiron site in both its diferric and diferrous forms from those of RNR-R2 and MMOH. The most striking of these is the redox-induced Glu97↔His56 ligand switching at Fe1 and the 1.8-Å movement of this iron in Rbr, which has no counterpart in either RNR-R2 or MMOH. In addition, the oxo bridge in the diferric RNR-R2 site is coordinated trans to the single bridging carboxylate and cis to the two His ligands, which is the reverse of the oxo bridge disposition in Rbr_{ox} (cis to the two bridging carboxylates and trans to the single His131 ligand). The diferric MMOH site contains no oxo bridge but rather two bridging solvent ligands, modeled as hydroxo and aqua, the latter disposed trans to the two His ligands.[56] The Rbr diiron site retains the same two

(44) Armstrong, G. D.; Sykes, A. G. *Inorg. Chem.* **1986**, *25*, 3514−3516.
(45) Nordlund, P.; Eklund, H. *Curr. Opin. Struct. Biol.* **1995**, *5*, 758−766.
(46) Stillman, T. J.; Hempstead, P. D.; Artymiuk, P. J.; Andrews, S. C.; Hudson, A. J.; Treffry, A.; Guest, J. R.; Harrison, P. M. *J. Mol. Biol.* **2001**, *307*, 587−603.
(47) Harrison, P. M.; Hempstead, P. D.; Artymiuk, P. J.; Andrews, S. C. In *Iron transport and storage in microorganisms, plants, and animals*; Sigel, A., Sigel, H., Eds.; Metal Ions in Biological Systems 35; Marcel Dekker: New York, 1998; pp 435−477.
(48) Frolow, F.; Kalb Gilboa, J.; Yariv, J. *Nat. Struct. Biol.* **1994**, *1*, 453−460.
(49) LeBrun, N. E.; Thomson, A. J.; Moore, G. R. *Struct. Bonding (Berlin)* **1997**, *88*, 103−138.
(50) Yang, X.; Le Brun, N. E.; Thomson, A. J.; Moore, G. R.; Chasteen, N. D. *Biochemistry* **2000**, *39*, 4915−4923.
(51) Guex, N.; Diemand, A.; Peitsch, M. C. *Trends Biochem. Sci.* **1999**, *24*, 364−367.
(52) Hogbom, M.; Huque, Y.; Sjoberg, B. M.; Nordlund, P. *Biochemistry* **2002**, *41*, 1381−1389.
(53) Logan, D. T.; Su, X. D.; Aberg, A.; Regnstrom, K.; Hajdu, J.; Eklund, H.; Nordlund, P. *Structure* **1996**, *4*, 1053−1064.
(54) Nordlund, P.; Eklund, H. *J. Mol. Biol.* **1993**, *232*, 123−164.
(55) Eriksson, M.; Jordan, A.; Eklund, H. *Biochemistry* **1998**, *37*, 13359−13369.
(56) Whittington, D. A.; Lippard, S. J. *J. Am. Chem. Soc.* **2001**, *123*, 827−838.
(57) Elango, N.; Radhakrishnan, R.; Froland, W. A.; Wallar, B. J.; Earhart, C. A.; Lipscomb, J. D.; Ohlendorf, D. H. *Protein Sci.* **1997**, *6*, 556−568.
(58) Rosenzweig, A. C.; Brandstetter, H.; Whittington, D. A.; Nordlund, P.; Lippard, S. J.; Frederick, C. A. *Proteins* **1997**, *29*, 141−152.

Scheme 1

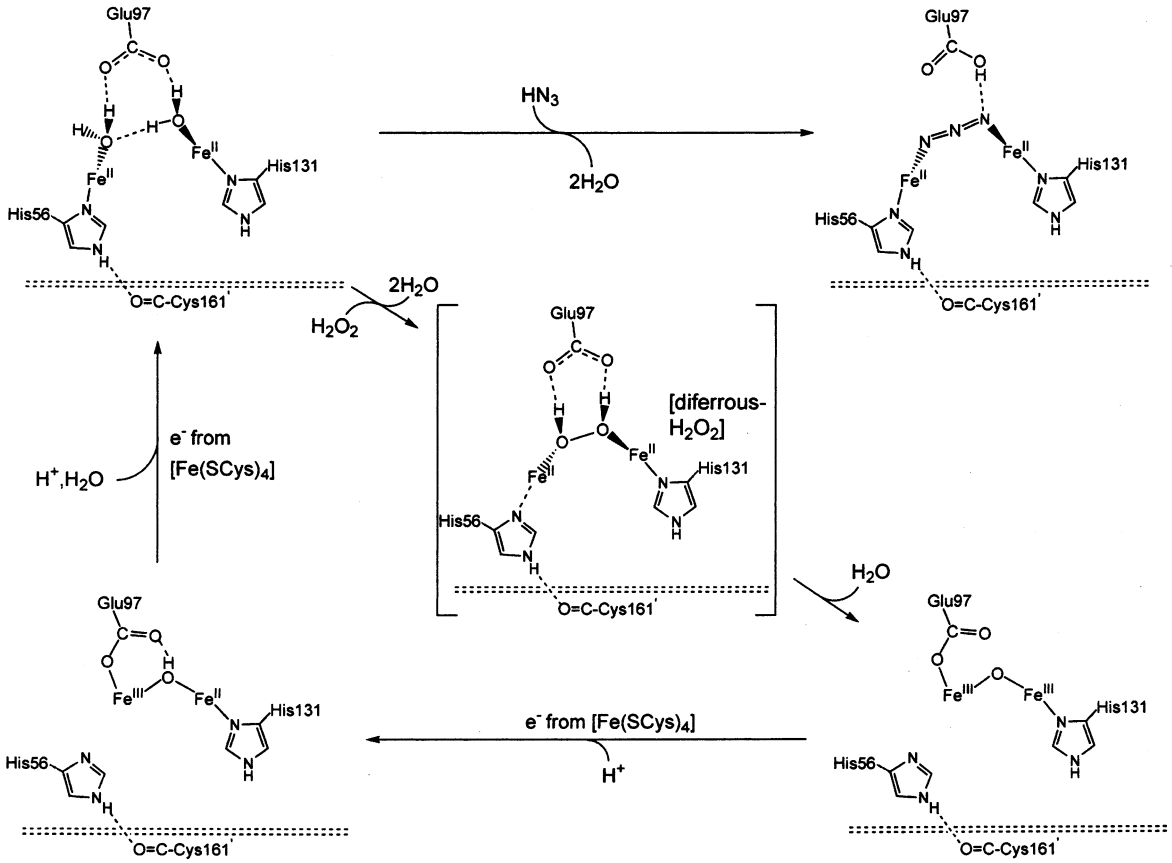

bidentate bridging carboxylate ligands in both diferric and diferrous forms. The diferric sites of RNR-R2 and MMOH, on the other hand, each contain only a single carboxylate bridge (also bidentate), which upon reduction to the diferrous forms is joined by a second bridging carboxylate that enters from a terminal coordination position. The Rbr diiron site shows no evidence for a monodentate bridging carboxylate, unlike diferrous MMOH. The bridging carboxylate ligation upon diferric/diferrous interconversion is, thus, relatively inflexible in Rbr.

The relative structural rigidity of the diferrous Rbr_{red} site indicated by the lower Fe1 and Fe2 *B*-factors in Rbr_{red} vs Rbr_{ox} (vide supra) is also reflected in the essential absence of structural changes upon azide binding (cf. Figure 2, lower right). In the azide adduct of a pocket-mutated diferrous RNR-R2,[36] η^1-terminal coordination of azide to one of the irons induced a shift of one of the bridging carboxylate ligands from bidentate to μ-(η^2,η^1), a 0.4-Å shortening of the Fe1- - -Fe2 distance, and a change from four- to six-coordination of the azide-bound iron. Both Fe1 and Fe2 of the Rbr diiron site retain their six-coordination upon conversion from the diferric to the diferrous form, whereas the irons in RNR-R2 and MMOH change from six- to either four- or five-coordinate upon reduction. The approximate two-fold rotational symmetry noted above for the diferrous sites of both Rbr_{red} and $Rbr_{red}N_3$ is not duplicated in either RNR-R2 or MMOH.

In both Rbr_{ox} and Rbr_{red}, the Glu20 and Glu94 carboxylate ligands are each hydrogen-bonded to the hydroxyl group of a tyrosine residue, as depicted in Figure 3. Although not sequentially homologous to those in Rbr, RNR-R2 contains a tyrosine that is hydrogen-bonded to one of its terminal carboxylate ligands in the diferrous form (shown in Figure 7). Reaction of the diferrous site of RNR-R2 with O_2 produces a stable and functionally essential phenoxyl radical from this tyrosine side chain, whereas no stable tyrosyl radical has been reported for Rbr. Tyrosine side chains are not evident near the MMOH diiron site; a cysteine residue is instead found in the position analogous to the tyrosine in RNR-R2. A functional role for this conserved cysteine has been proposed[59] but not established. *D. vulgaris* Rbr contains no cysteine residues other than those of the [Fe(SCys)$_4$] site. Finally, unlike the buried diiron sites in RNR-R2 and MMOH, the diiron site of Rbr_{red} is readily solvent accessible, as can be seen from Figure 5.

Mechanistic Inferences. A mechanism for hydrogen peroxide reduction by the Rbr_{red} diiron site that is consistent with the new structural data described here is shown in Scheme 1. The first step consists of displacement of the coordinated solvent ligands by the entering hydrogen peroxide, forming a transient diferrous−hydroperoxo adduct. We had previously suggested a μ-η^1 peroxo geometry for this intermediate, based on solvent molecule positions in the 1RYT structure.[3] However, the relatively symmetrical and rigid Rbr_{red} diferrous site, the cis disposition of its only two solvent (i.e., labile) coordination sites, and the 4-Å Fe1- - -Fe2 distance would more readily accommodate coordination of hydrogen peroxide in a cis μ-η^2 fashion, as shown in Scheme 1. This coordination mode, in fact, mimics the cis μ-1,3 geometry of the coordinated azide in $Rbr_{red}N_3$.

A concerted process can then be readily envisioned in which transfer of one electron from each ferrous iron to its coordinated

(59) Feig, A. L.; Lippard, S. J. *Chem. Rev.* **1994**, *94*, 759−805.

hydroperoxo oxygen occurs concomitantly with O−O bond cleavage. This process would be rapidly followed by proton transfer from one oxygen to the other and loss of the latter oxygen as water. The remaining coordinated oxygen would form the oxo bridge in the resulting diferric site. The proton transfer from one coordinated hydrogen peroxide-derived oxygen to the other could be facilitated by the Glu97 carboxylate as it rotates into position to displace His56 as a ligand to the ferric Fe1. The Glu97 carboxylate rotation coupled with the incipient oxo ligand on ferric Fe2 (the His131-ligated iron in Scheme 1) would tend to draw the ferric Fe1 away from His56. Including the carboxylate of Glu97, there would be no net change in charge (−1) on the diiron site during this transformation. Electron transfer from the [Fe(SCys)$_4$] site across the subunit interface (cf. Figure 1) could, in principle, re-reduce the diiron site prior to formation of the oxo-bridged structure in Rbr$_{ox}$. Our stopped-flow kinetic studies[60] indicate, however, that upon mixing of hydrogen peroxide with Rbr$_{red}$, intramolecular [Fe(SCys)$_4$]-to-diiron site electron transfer occurs only after formation of the oxo-bridged diferric site. This intersite electron transfer leads to the antiferromagnetically coupled mixed-valent [Fe(II),Fe(III)] diiron site previously identified by EPR spectroscopy.[18,61]

The two symmetrically placed tyrosyl side chains, Tyr27 and Tyr102, that are hydrogen-bonded to terminal carboxylate ligands of the Rbr diiron site (cf. Figure 3) are conserved in all known Rbr amino acid sequences.[3] A Y27F *D. vulgaris* Rbr variant retained 30% of the wild-type peroxidase activity when measured as initial rates.[3] However, the Y27F variant also gradually lost its peroxidase activity during turnover. One function of these tyrosines may be to reverse Fenton-type chemistry[63] at the diferrous or mixed-valent [Fe(II),Fe(III)] site by formation of transient phenoxy radicals, thereby protecting Rbr from irreversible oxidative damage during peroxidase turnover. Such protection against "hyperoxidation" has been suggested for a similarly hydrogen-bonded tyrosyl residue during reaction of hydrogen peroxide with the dimanganese active site in pseudocatalases.[64] As mentioned earlier, we have detected little or no reaction of the diferric Rbr site with hydrogen peroxide.[3] In any case a concerted two-electron transfer from the diferrous site to the μ-1,2 H_2O_2 (cf. Scheme 1) would minimize Fenton-type chemistry, i.e., the one-electron reduction of H_2O_2 to produce OH$^\bullet$.

Although the MMOH diiron site can function as an NADH peroxidase in the absence of hydrocarbon substrates,[65] and may do so at the expense of NADH oxidase activity (i.e., the competing reduction of O_2), the reported NADH peroxidase turnover for MMOH is at least 100-times slower than that for Rbr.[9] The relatively rapid turnover of hydrogen peroxide by Rbr may be due to the much greater solvent exposure and polarity of its diiron site, which would facilitate entry and exit of the polar, protic substrate (hydrogen peroxide) and product (water). On the other hand, the reactions of excess dioxygen with the diferrous sites of RNR-R2 and MMOH are at least 1000-times faster than that with Rbr$_{red}$[4,66] (although the MMOH reaction is "gated", requiring an additional protein component for facile reaction with O_2). The relatively solvent-inaccessible diferrous sites and their coordinative unsaturation in RNR-R2 and MMOH may facilitate their well-established inner-sphere reactions with dioxygen.[66] In the solvent-exposed, Glu97-lined ligand binding pocket at the diferrous site Rbr$_{red}$, on the other hand, dioxygen may not be able to compete with water for coordination to iron, leading to a slower, outer-sphere reaction with dioxygen.[67] This solvent exposure, the relatively inflexible bridging carboxylate ligation, the relatively ordered diferrous irons with nearly superimposable coordination spheres, the redox-induced iron movement, and the Glu↔His ligand switching are all unique features of the Rbr diiron site revealed by the structures reported here. These structures should, therefore, facilitate delineation of the dioxygen vs hydrogen peroxide reactivity of this unique member of the non-heme, non-sulfur class of diiron enzymes.

Acknowledgment. This work was supported by the National Institutes of Health (GM40388 to D.M.K.).

Supporting Information Available: X-ray data for Rbr$_{ox}$, Rbr$_{red}$, and Rbr$_{red}$N$_3$ (CIF). This material is available free of charge via the Internet at http://pubs.acs.org.

JA026587U

(60) Jin, S.; Phillips, R.; Coulter, E. D.; Kurtz, D. M., Jr., unpublished.
(61) ENDOR studies (ref 62) detect only one histidine ligand to the mixed-valent Rbr diiron site, which, on the basis of the Rbr$_{ox}$ structure, we assign to His131.
(62) Smoukov, S. K.; Davydov, R. M.; Doan, P. E.; Sturgeon, B.; Hoffman, B. M.; Kurtz, D. M., Jr. *Biochemistry* **2002**, submitted.
(63) Branchaud, B. P. In *Interrelations between free radicals and metal ions in life processes*; Sigel, A., Sigel, H., Eds.; Metal Ions in Biological Systems 36; Marcel-Dekker: New York, 1999; pp 79−102.
(64) Barynin, V. V.; Whittaker, M. M.; Antonyuk, S. V.; Lamzin, V. S.; Harrison, P. M.; Artymiuk, P. J.; Whittaker, J. W. *Structure (Cambridge)* **2001**, *9*, 725−738.
(65) Gassner, G. T.; Lippard, S. J. *Biochemistry* **1999**, *38*, 12768−12785.
(66) Wallar, B. J.; Lipscomb, J. D. *Chem. Rev.* **1996**, *96*, 2625−2657.
(67) Perhaps for the same reasons, we have been unable to detect any reaction of Rbr$_{red}$ with nitric oxide, in contrast to RNR-R2 and MMOH, whose diferrous sites readily react with nitric oxide (refs 68 and 69).
(68) Haskin, C. J.; Ravi, N.; Lynch, J. B.; Munck, E.; Que, L., Jr. *Biochemistry* **1995**, *34*, 11090−11098.
(69) Coufal, D. E.; Tavares, P.; Pereira, A. S.; Hyunh, B. H.; Lippard, S. J. *Biochemistry* **1999**, *38*, 4504−4513.